Soft Matter

PAPER

View Article Online
View Journal | View Issue

Cite this: *Soft Matter*, 2018, **14**, 2170

Importance of matrix inelastic deformations in the initial response of magnetic elastomers

Pedro A. Sánchez, *[ab] Thomas Gundermann, [c] Alla Dobroserdova, [b] Sofia S. Kantorovich [ab] and Stefan Odenbach[c]

Received 1st December 2017,
Accepted 9th February 2018

DOI: 10.1039/c7sm02366a

rsc.li/soft-matter-journal

Being able to predict and understand the behaviour of soft magnetic materials paves the way to their technological applications. In this study we analyse the magnetic response of soft magnetic elastomers (SMEs) with magnetically hard particles. We present experimental evidence of a difference between the first and next magnetisation loops exhibited by these SMEs, which depends non-monotonically on the interplay between the rigidity of the polymer matrix, its mechanical coupling with the particles, and the magnetic interactions in the system. In order to explain the microstructural mechanism behind this behaviour, we used a minimal computer simulation model whose results evidence the importance of irreversible matrix deformations due to both translations and rotations of the particles. To confirm the simulation findings, computed tomography (CT) was used. We conclude that the initial exposure to the field triggers the inelastic matrix relaxation in the SMEs, as particles attempt to reorient. However, once the necessary degree of freedom is achieved, both the rotations and the magnetisation behaviour become stationary. We expect this scenario not only to be limited to the materials studied here, but also to apply to a broader class of hybrid SMEs.

1 Introduction

The embedding of solid magnetic colloidal particles, with typical sizes ranging from tens of nanometres to a few hundreds of micrometres, within elastic matrices of crosslinked polymers is the basis of an important class of smart materials whose physical properties, like their shape or their mechanical and rheological behaviour, can be tuned by means of external magnetic fields.[1–3] This type of composite material includes magnetic gels, in which the polymer matrix remains swollen by a significant amount of background liquid,[4–11] and soft magnetic elastomers (SMEs), also known as magnetorheological elastomers (MREs), which are magnetic rubber-like solid materials.[3,12–18] In both cases there is a coupling between the magnetic response and self-assembly behaviour of the embedded magnetic particles and the structural properties of the polymer matrix. This provides such materials with striking properties of great technological interest, including a very quick and strong response to external stimuli, giant reversible deformations, controllable elastic moduli and strongly anisotropic behaviour.[1,19] Such combination of properties has highlighted magnetic gels and elastomers as novel components in many technological applications. For instance, SMEs have been suggested or used for the design of adaptive damping devices, vibrational absorbers, stiffness tunable mounts, soft actuators and micromanipulators, force sensors and artificial muscles.[14,20–25]

Current experimental techniques for the synthesis of magnetic gels and elastomers offer different mechanisms for the embedding of the magnetic particles within the polymer matrix. In one of the main cases, the magnetic particles simply become physically trapped into hollow 'pockets' of the matrix during the synthesis process. Under these conditions, the particles experience a translational constraint imposed by the 'walls' formed by the surrounding mesh of polymers, while keeping a higher orientational freedom in case the volume of the cavity is larger than those of the magnetic particles.[1] In the second case, the surface of the magnetic particles is functionalised, allowing the formation of chemical bonds with the polymers. In this way, the particles play the role of network crosslinkers and not only their translations, but also their rotations are constrained by a mechanical coupling with the polymer matrix.[7–9] Finally, in the third case there is no chemical binding between the particles and the matrix but the latter is so compact that both translations and rotations might be hindered, especially when the particles are large and/or anisotropic. In all cases, the mechanical coupling between the magnetic particles and the polymer matrix makes the field-induced microscopic displacements and reorientations of the former responsible for the macroscopic deformations of the material.

The macroscopic response produced by the field-induced self-assembly of magnetic micro- and nanoparticles is a phenomenon

[a] *University of Vienna, Sensengasse 8, Vienna, 1090, Austria. E-mail: pedro.sanchez@univie.ac.at*
[b] *Ural Federal University, Lenin av. 51, Ekaterinburg, 620000, Russia*
[c] *Technische Universität Dresden, Institute of Fluid Mechanics, Dresden, D-01062, Germany*

extensively studied in another class of soft magnetic materials: the dispersions of magnetic particles in inert carrier liquids known as magnetic fluids. It is well known that magnetic particles in dispersion tend to form chain-like arrangements under applied external fields. These chains tend to follow the field lines by keeping a head-to-tail orientation of the magnetic moments of their particles.[26,27] The same type of field-induced rearrangement takes place for the magnetic particles embedded in magnetic gels and elastomers,[3,28,29] but in this case the mechanical constraints imposed by the polymer matrix may hinder to some extent the particle rearrangements. Basically, the local displacements and reorientations of the particles induced by external fields tend to produce deformations of the polymer matrix with an associated mechanical energy penalty. This phenomenon, known as magneto-dipolar striction (MDS),[30] is fundamental in the behaviour of these materials. In particular, as long as the elastic limit of the polymer matrix is not exceeded, such deformations tend to be spontaneously reverted after field removal. In this way, these materials can exhibit important shape memory properties.[2,28,31]

The reversibility of the changes in the shape and mechanical properties of magnetic gels and elastomers is crucial for many prospective applications. For this reason, the study of their behaviour in elastic regimes has been the subject of most research studies to date. However, the characterisation of their irreversible deformations under strong enough external fields is also essential from both perspectives, their fundamental understanding and the design of technological applications. Related to this important aspect, very recent experimental measurements have shown that a novel type of hybrid magnetic elastomer, obtained by embedding a mixture of magnetically soft and hard particles within the polymer matrix, may exhibit certain unconventional features: among other properties that provide important technological advantages, these materials can exhibit a significant nonelastic behaviour when still freshly synthesised. In particular, they display a substantial change in their magnetic response during their first exposure to external fields.[32] This is experimentally evidenced by consecutive measurements of conventional magnetisation loops: in some cases a notable difference in the shape of the first hysteresis loop can be observed, particularly in the second half of the backward curve, when compared to the next ones (see, for instance, Fig. 4(c) in ref. 32). In addition, in these magnetically hybrid materials the magnetisation loops tend to show some bias, with different values of the forward and backward coercivities.[32,33] A reasonable explanation for this behaviour is that it corresponds to the signature of irreversible internal changes in the material induced by the first-time application of an external field, but the nature of such changes is still unclear. Another important effect might be the complex interplay between the magnetically hard and soft particles. Some efforts to understand this phenomenon that do not take into account inelastic processes have already been made: a very recent theoretical study presented a microscale two-dimensional model of SMEs, based on a magnetomechanical continuum formulation, which predicts a large difference in the first magnetisation loop as a consequence of the strain energy stored in the elastic matrix in the initial magnetisation curve.[34] Even this model naturally includes the detailed magnetic interactions between close particles, the predicted difference is much larger than the experimental one, which suggests that the relevant underlying physical mechanisms might not be fully captured by this approach. Therefore, the contribution of eventual irreversible deformations of the matrix to the experimental behaviour remains to date as an open question. Unfortunately, even though it is already possible to observe the deformations of the matrix by means of confocal microscopy techniques,[35] the available experimental methods are not accurate enough to provide a direct observation of its irreversible microstructural changes. This makes the study of such irreversible deformations and their effects particularly challenging. Another complication for the study of hybrid SMEs is the limited resolution in the observation of the magnetic particles. Current X-ray tomography techniques are able to image relatively large solid particles, such as the magnetically hard ones used in these materials. The imaging of the smaller, magnetically soft particles used in the aforementioned hybrid SMEs, with typical sizes not larger than 5 μm, requires an increase of their resolution power that is still under development. Alternatively, one could also create hybrid SMEs using magnetically soft particles large enough to be observable with available experimental methods, but in this case it would be hard to distinguish them from the magnetically hard ones.

The difficulties discussed above suggest the use of a reductionist strategy in order to unveil the role of inelastic matrix deformations in the distinctive first magnetisation loop originally observed for hybrid SMEs. With this goal, here we study experimentally and theoretically a simpler SME material, composed of only relatively large magnetically hard particles. In this way, we avoid the complex magnetic interactions between heterogeneous particles to focus on the analysis of elastic and inelastic microstructural deformations induced by the external field. This analysis includes several results. First, we provide the first experimental evidence of simple SMEs also showing a difference in their first magnetisation loop, obtained from measurements using a vibrating sample magnetometer (VSM), proving that this behaviour is not exclusive of hybrid materials. Second, we study by means of computer simulations with a minimal model of SMEs if irreversible deformations of the matrix alone can reproduce the experimental loops, showing that a good qualitative agreement is obtained when such deformations increase both the translational and rotational freedom of the magnetic particles. Finally, we characterise experimentally the movements of the particles as a response to the applied field using micro-computed tomography imaging (Xμ-CT), showing that they are consistent with the theoretical assumptions.

This paper is organized as follows. First, in Section 2.1, the experimental approach is presented. Section 2.2 describes the theoretical modeling approach. The results are presented in Section 3. Finally, conclusions and outlook are discussed in Section 4.

2 Methods

2.1 Experimental approach

In the last few years a new method to investigate soft magnetic hybrid materials containing microparticles was developed.

Using micro computed tomography (Xμ-CT) with the combination of a magnetic field setup, the microstructure of such SME materials could be observed and analysed analytically.[29,36–38] The advantage of this method is the possibility of three-dimensional analysis of opaque materials within a resolution of a few microns and a comparison of microstructural changes under the influence of external stimuli like a magnetic field,[29] which is of particular interest in this study.

Considering the SME Material Xμ-CT is a tool to analyze particle structures[36,37] up to a single particle detection[29,35,38] inside such SME materials. This leads to statements about particle distribution[39] and particle motion under the influence of an external magnetic field.[29,35,38]

Of great importance when considering such SME materials is the effect of the microstructural changes on macroscopic behaviours such as the mechanical response and the magnetic properties of the material. To establish this relationship, magnetic measurements of the samples using a vibrating sample magnetometer (VSM) have been carried out with respect to the CT-scans to enable a physical description of the material. Particular hysteresis effects which were already found in a previous study[32] are to be explained by using this method. For this purpose, a VSM Lake Shore 7404 was used to perform the magnetic measurements.

Three different samples containing 5 vol% of magnetically hard NdFeB microparticles dispersed isotropically in an elastomeric matrix ELASTOSIL RT 623 A/B by Wacker Corp. Germany were produced. The samples were of a cylindrical shape with a diameter of 4 mm and a height of 4 mm. A silicon oil with a viscosity of 100 000 Pa s was used to adjust the elastic modules and to avoid sedimentation. Thereby a sample with a tensile module of E = 30 kPa (SME1), a sample with a tensile module of E = 80 kPa (SME2) and a sample with a tensile module of E = 900 kPa (SME3) were produced. In contrast to the work in ref. 32, no magnetically soft particles were added to the samples.

To carry out the CT investigations we used a home build Xμ-CT System based on a nano-focus tube with a maximum acceleration voltage of 160 kV and a detector with a photodiode array of 2940 × 2304 (horizontal × vertical) pixels. The sample was placed on a movable sample holder between the X-ray tube and detector. The sample holder consists of two cylindrical permanent magnets which were mounted displaceable and could generate a homogeneous field parallel to the direction of gravity in the range of B = 0–400 mT. This enables investigations of cylindrical samples with a height of 4 mm and a diameter of 4 mm within a magnetic field with a homogeneity of more than 95% in a radial and axial direction.[40] The temperature during the CT investigations was kept constant at 20 °C and projection images were generated by rotating the sample with a 0.25° angular increment for a tube current of 170 μA and an acceleration voltage of 90 kV. The exposure time was varied between 0.8 s and 1.0 s to achieve the highest image quality. The magnification was 20, which results in a resolution of 1 pixel = 2.5 μm. The reconstruction of the CT scans was carried out using home-made software. The evaluation of the reconstructed images was carried out by using MATLAB 7.10.0 software within the toolbox DIPimage. In order to separate the particles from the surrounding matrix, a threshold was set with respect to the known particle volume concentration in the sample. After separation, the particles were identified individually by using a watershed algorithm.[41] This separation of clustered particles leads to the possibility to calculate the size, surface area, position and main axes, including their directions, for each single particle. An example of the evaluation process results is shown as an image of the separated particles in a reconstructed CT measurement in Fig. 1(a). One can see that the particles have a flake like shape and a high polydispersity. The mean size of the particles was determined by sieving and has resulted in a range between 10 μm and 100 μm. Due to the possibility of calculating the size of the particles, a size distribution could be determined by an approximation of the particles by a sphere. The size distribution is shown in Fig. 1(b) and it confirms the size-range that was estimated from the sieving. The image processing allows us to calculate the direction of the major axes relative to a given vector. In our CT setup, the magnetic field is always vertical. The rotation of the particles is given by the angle between the longest major axis and the direction of the field. In order to analyse the reorientations of the particles during magnetisation–demagnetisation, CT scans at different points of the hysteresis loops were performed.

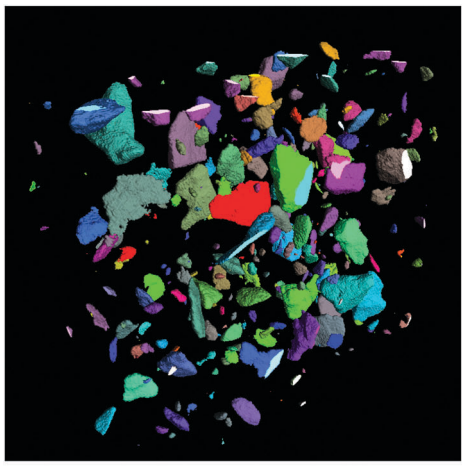

(a)

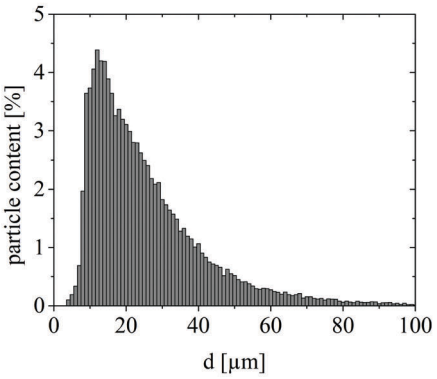

(b)

Fig. 1 (a) Segmented flake-like shaped hard magnetic particles inside an elastomeric matrix within a concentration of 5 vol% after image processing. (b) Size distribution of the particles by approximating the particles with a sphere.

2.2 Theoretical modelling approach

Computer simulations have been one of the main tools used to support the theoretical modelling of magnetic gels and elastomers, together with mean-field and continuum analytical theories,[30,42–46] for more than one decade already. Despite the appearance of promising experimental observation techniques,[33] the understanding of the field-induced local rearrangements of the embedded particles and their impact on the macroscopic response of these materials can still largely benefit from simulations. In general, simulation models for these systems are based on coarse-grained approaches. With only a few exceptions,[47] the embedded magnetic particles are modelled as beads with point magnetic dipoles, whereas the polymer matrix has been represented with different levels of detail. In most simple approaches, the matrix is simulated implicitly and affine deformations are assumed.[48,49] The simplest explicit representations of the matrix are based on networks of elastic springs in which the magnetic beads act as crosslinkers.[47,50–54] Finally, some studies represent explicitly the chain-like structure of the individual polymers forming the matrix by means of bead-spring models, in which polymer blobs or individual monomers are modelled as beads bonded by elastic springs.[55–58]

Here, we model a simple magnetic elastomer system filled with magnetically hard particles, incorporating a novel minimal representation of the effects of inelastic deformations of the polymer matrix on the magnetic response.

2.2.1 Minimal elastomer model: magnetic and interparticle interactions. We simulate the magnetic particles as identical ideal spheres with a point magnetic dipole, $\vec{\mu}$, located at their centres. Since here we are only interested in the effects of the mechanical constraints produced by the polymer matrix, we consider the modulus of the dipole of each particle to be fixed to a certain value, $\mu_i = \|\vec{\mu}_i\| = \mu$. This means that μ is not affected by the fields of other particles or any applied external field. Therefore, each pair of dipolar spheres experiences the conventional dipole–dipole pair interaction:

$$U_{\mathrm{dd}}(ij) = -3\frac{(\vec{\mu}_i \cdot \vec{r}_{ij})(\vec{\mu}_j \cdot \vec{r}_{ij})}{r^5} + \frac{(\vec{\mu}_i \cdot \vec{\mu}_j)}{r^3}, \quad \vec{r}_{ij} = \vec{r}_i - \vec{r}_j, \qquad (1)$$

where $\vec{r}_{ij}$ is the displacement vector between the centres of the interacting spheres i and j, and $\vec{\mu}_i$, their respective magnetic dipoles. As mentioned above, this type of anisotropic interaction leads to a strongly directional self-assembly of particles in magnetic fluids, gels and elastomers.

In case a uniform external magnetic field, $\vec{H}$, is applied, every particle i also experiences the effect of the Zeeman interaction:

$$U_{\mathrm{H}}(i) = -\vec{\mu}_i \cdot \vec{H} \qquad (2)$$

The steric repulsions between the magnetic particles are modelled by a truncated and shifted Lennard-Jones (LJ) interaction, also known as Weeks–Chandler–Andersen (WCA) potential.[59] This is defined as:

$$U_{\mathrm{WCA}}(r) = \begin{cases} U_{\mathrm{LJ}}(r) - U_{\mathrm{LJ}}(r_{\mathrm{cut}}), & r < r_{\mathrm{cut}} \\ 0, & r \geq r_{\mathrm{cut}} \end{cases}, \qquad (3)$$

where r is the modulus of the displacement vector $\vec{r}_{ij}$ defined above, $r = |\vec{r}_{ij}|$, $U_{\mathrm{LJ}}(r)$ is the conventional LJ potential, $U_{\mathrm{LJ}}(r) = 4\varepsilon[(\sigma/r)^{12} - (\sigma/r)^6]$, r_{cut} is the cutoff distance at which it is truncated, σ the characteristic diameter of the particles and ε corresponds to the energy scale of the steric interactions in the system. The WCA potential, frequently used in coarse-grained dynamics simulations, allows us to represent purely repulsive isotropic interactions by taking $r_{\mathrm{cut}} = 2^{1/6}\sigma$.

Finally, we chose a minimal implicit representation for the constraints imposed by the polymer matrix on these magnetic particles: for any system formed by N magnetic beads, we assume every one of them to be trapped by the matrix and mechanically forced to remain within a limited region of the space around its initial position, corresponding to a local elastic equilibrium. For simplicity, such initial positions are placed randomly in space with a given number density, ρ. At this point, in order to complete the description of our modelling approach, we have to distinguish between the two aforementioned mechanisms of coupling between the particles and the matrix.

2.2.2 Minimal elastomer model M1: translational constraints. In the simplest case only particle translations are constrained, whereas rotations are free. For this scheme, that from now on we will refer to as model M1, we connect the centre of each magnetic particle to one end of a harmonic spring. The opposite end of the spring is fixed to a point of space, or anchoring point, corresponding to the equilibrium position of the particle. Therefore, the spring hinders only the translations of the particle with the potential

$$U_{\mathrm{C}}(r) = \frac{1}{2}Kr^2, \qquad (4)$$

where K is the energy scale of the constraint and r is the distance between the anchoring point and the centre of the particle. Fig. 2(a) shows a schematic representation of this M1 elastomer model.

2.2.3 Minimal elastomer model M2: translational and rotational constraints. In the second case, not only translations but also the rotations of the magnetic particles are hindered by the polymer matrix. To represent this effect, we use a second model, M2, in which the single spring connected to each particle's centre is replaced by two analogous springs, also governed by eqn (4). Each one of these springs has one of their ends connected to a point on the particle's surface, located respectively at the projection points of the head and the tail of the particle's magnetic dipole. The opposite spring ends are also fixed to two different anchoring points in space, separated

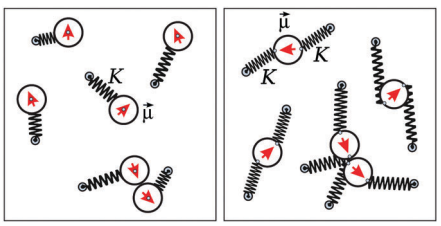

Fig. 2 (a) Model M1: translational constraints. (b) Model M2: translational and rotational constraints.

by a relative distance a. By taking the same elastic constant for both springs of a given particle, the local equilibrium position corresponds to both the perfect alignment of the dipole with the head and tail anchoring points and its location at a distance $a/2$ from them. In this way, displacements or rotations from this local equilibrium configuration are both penalised by the stretching of at least one of the springs. Fig. 2(b) shows a scheme of the resulting elastomer model. This coupling between the orientation of the magnetic particle and the matrix polymers grafted to its surface is inspired by the bonding model used for polymer crosslinked ferromagnetic nanoparticle filaments.[60,61]

So far, we have defined the models for the elastic behaviour of the mechanical constraints affecting the magnetic particles in a elastomer. The last ingredient in our minimal modelling approach is to take into account the inelastic deformations induced by the application of external fields.

2.2.4 Modelling inelastic deformations. Before describing the details of the modelling of the inelastic deformations in each system, we first introduce a general assumption: we consider these inelastic deformations to occur only when an external field of a given strength and direction is applied to the system for the first time. This means that, when performing consecutive magnetisation measurements, the system is supposed to experience irreversible changes only during the initial magnetisation curve—when the field grows from 0 to its maximum value, H_{max}, for the first time—and along the second half of the first downward magnetisation curve—when the field inverts its orientation for the first time, changing from 0 to $-H_{max}$. The rationale behind this assumption is that the field-induced local displacements and reorientations of the magnetic particles are able to produce those permanent deformations in the surroundings of the polymer matrix that favour both, their alignment with the field and their possible assembly with near particles. In general, this occurs by means of some mechanism that increases or redistributes the particles' degrees of freedom. For instance, polymer crosslinkers may break when strong enough torques on crosslinked particles are induced by the field, and/or walls of polymer hollow 'pockets' separating close magnetic particles may permanently deform. After creating "pathways" to optimise dipolar, Zeeman and elastic energies, the particles on further magnetisation loops will simply follow them, thus the system is assumed to keep an elastic regime. In our simulations, this behaviour has been modelled by switching on and off inelastic deformations at the suitable parts of the magnetisation curves.

For M1, every time the distance between the centre of a particle and its anchoring point, r, becomes larger than a given threshold, $r > r_{th}$, a shift of the anchoring point towards the particle centre is performed with a certain arbitrary probability,

$$P_{M1}^{shift} = p_s, \quad (5)$$

so that the shift may reduce the extension of the spring constraining the particle. We chose the shift to be randomly selected between 0 and $\sigma/2$, and the threshold extension of any given spring with elastic constant K to be

$$r_{th} = \left(\frac{2\mu^2}{K}\right)^{1/2}, \quad (6)$$

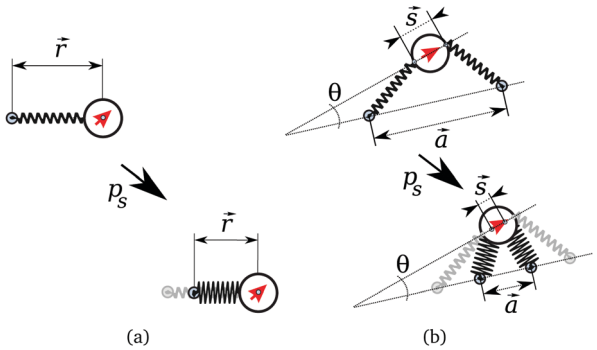

Fig. 3 Inelastic deformations for models M1 (a) and M2 (b), represented as shifts of the anchoring points of the springs that reduce their stretching.

that corresponds to the value of r at which the elastic and the pair dipole–dipole energies become similar. Fig. 3(a) shows a scheme of this shifting procedure. With this approach, we assume that large degrees of stretching of the constraining springs will mainly occur due to the effects of the particles' field-induced assembly, so that the shifts of the anchoring points will tend to ease such assembly in subsequent exposures of the system to the same conditions.

Even based on the same strategy, inelastic relaxations of the rotational constraints in model M2 require a slightly more sophisticated approach. In this case, the criterium to attempt an irreversible change in the constraints of a given particle is a continuous distribution that grows with the misalignment of the dipole with respect to the orientation corresponding to the mechanical equilibirum of the springs. This misalignment is measured by θ, that is defined as the angle between the dipole moment of the particle, $\vec{\mu}$, and the displacement vector between the anchoring points of the springs corresponding to the tail and the head of the dipole, $\vec{a} = \vec{r}_{head} - \vec{r}_{tail}$, as depicted in the scheme of Fig. 3(b). In general, angle θ will tend to grow statistically with the strength of the external field, $H = \|\vec{H}\|$, due to the torque produced by the Zeeman interaction on the magnetic dipole of the particles, $\vec{\tau} = \vec{\mu} \times \vec{H}$. We take the modulus of this torque, nomalised with the saturation field strength, H_{max}, as the main part of the probability distribution for performing an irreversible relaxation of the constraints, with an added arbitrary prefactor, p_s, as free tuning parameter. Therefore, the final expression is

$$P_{M2}^{shift} = p_s \left|\frac{H}{H_{max}}\right| \sin\theta. \quad (7)$$

In this case the irreversible change consists of shifting at the same time the four fixed ends of the springs in order to decrease symmetrically and in the same proportion the displacement vector between the anchoring points, $\vec{a}$, and the displacement vector between the points at which the springs are attached to the particle, $\vec{s}$. This decrease of the distances $\vec{a}$ and $\vec{s}$ increases the particle freedom to move and rotate respectively. The relative change in the modulus of these vectors performed in any succesful shifting attempt is given by

$$\frac{\Delta\vec{a}}{\vec{a}} = \frac{\Delta\vec{s}}{\vec{s}} = \delta, \quad (8)$$

where δ is a random value between 0 and 1. Fig. 3(b) provides a scheme of this irreversible shifting procedure. Note that it makes $\vec{a}$ and $\vec{s}$ tend to zero. In that limit, the anchoring points of the springs reach a common position in the simulation box and their attachment points to the particle become equally located at its centre. This means that the shifting procedure in model M2 makes the constraints tend towards becoming analogous to the ones defined for M1, with the only difference being that the single spring attached to the centre of each particle in M1 is here replaced by two identical overlapping springs acting on the same particle.

2.2.5 Simulation method. In order to analyse the magnetic response of the elastomer models introduced above, we performed extensive molecular dynamics simulations. It is important to underline that here we do not aim to characterise the dynamics, nor the thermodynamic equilibrium properties of the systems we simulate. Here we are only interested in the changes of the overall magnetisation as a response to variations of the external field and its interplay with the elastic constraints, including the irreversible initial relaxations of the latter.

In molecular dynamics simulations with coarse-grained models like these, it is usual to use a Langevin thermostat in order to approximate statistically the effects of the degrees of freedom neglected by the coarse-grained approach,[62] particularly the thermal fluctuations of the background fluid. Such fluctuations are very relevant in magnetic fluids and gels, in which the background fluid is a liquid. In elastomers, that are dry materials, thermal fluctuations at room temperature can be considered negligible in front of the magnetoelastic interactions. Since the latter are the only focus of our study, we basically need to perform athermal simulations. However, it might be still useful to keep some little thermal fluctuations in the simulation of these systems to favour their mechanical relaxation, because the strongly simplified representation of the effects of the polymer matrix, that ignores any long range mechanical coupling, makes them prone to kinetic trapping. Therefore, we chose to use a Langevin thermostat with a relatively low temperature.

In our simulations, we used an arbitrary system of reduced units. Note that the qualitative nature of our analysis makes the values we assign to the different parameters irrelevant when considered individually. Only their ratios, that determine the relative strengths of the interactions, are relevant for our purpose. In particular, we chose to measure lengths in units of the diameter of the particles, $\sigma = 1$. The energy scale of the magnetic interactions is defined by an arbitrary value of the minimum sampled Zeeman energy of each particle, defined by (2), that corresponds to the maximum absolute value of the saturation fields we apply during the magnetisation loops and the magnetic moment assigned to the dipoles. The chosen values for such magnitudes are, respectivley, $U_H^{\min} = -60$, $H^{\max} = 30$ and $\mu = 2$. For all sampled systems a random elastic constant, K_i, is assigned to each individual (M1) or pair (M2) of springs that anchor every particle i according to (4). This random value is taken from a Normal distribution with mean α and standard deviation s^2, $N(\alpha,s^2)$, that is defined to span over a fixed arbitrary interval $[K_{\min}, K_{\max}]$. This is carried out by taking $\alpha = (K_{\min} + K_{\max})/2$, $s = (K_{\max} - K_{\min})/6$ and rejecting all values that do not lie within the chosen interval during the random assignation procedure. In any case the minimum and maximum values of K_i we sampled are, respectively, $K_{\min} \geq 1$ and $K_{\max} \leq 30$. For the case of the model M2 systems, we chose the initial separation between anchoring points, defined for expressions (7) and (8), to be $|\vec{a}| = 5$. We chose the thermal energy in our simulated systems to be much lower than those associated with the magnetoelastic interactions by taking a reduced temperature of $T = 10^{-4}$. Finally, for the sake of simplicity, we chose the prefactor of the soft core steric interactions defined by (3) to be $\varepsilon = 1$. This latter choice is loosely connected to the rest of the energy scales we defined above, since the purpose of interaction (3) here is only to keep a minimum centre-to-centre distance between particles not much lower than their diameters, $\sigma = 1$. Therefore, any higher value for ε would also serve this purpose.

The Langevin dynamics method adds to the Newtonian equations of motion stochastic and friction terms that satisfy the usual fluctuation–dissipation relationships. In particular, the Langevin translational and rotational equations of motion governing the dynamics of a particle i are

$$m_i(\mathrm{d}\vec{v}_i/\mathrm{d}t) = \vec{F}_i - \Gamma_{\mathrm{T}}\vec{v}_i + \vec{\xi}_{i,\mathrm{T}} \quad (9)$$

and

$$\vec{I}_i\cdot(\mathrm{d}\vec{\omega}_i/\mathrm{d}t) = \vec{\tau}_i - \Gamma_{\mathrm{R}}\vec{\omega}_i + \vec{\xi}_{i,\mathrm{R}}, \quad (10)$$

where $\vec{F}_i$ and $\vec{\tau}_i$ are the total force and torque acting on the particle, m_i its mass and $\vec{I}_i$ its inertia tensor. Finally, Γ_{T} and Γ_{R} are the translational and rotational friction constants, and $\vec{\xi}_{i,\mathrm{T}}$ and $\vec{\xi}_{i,\mathrm{R}}$ are the Gaussian random force and torque, respectively. Since we are not interested in the system dynamics, the choice of friction constants can be arbitrary. We take $\Gamma_{\mathrm{T}} = 1$ and $\Gamma_{\mathrm{R}} = 3/4$, which are known for providing a fast system relaxation in this type of simulation.[63,64] For the inertia tensors, $\vec{I}_i$, the identity matrix was taken. In order to avoid finite size effects, we simulated a pseudo-infinite system by using 3-D periodic boundaries. Due to the long range nature of the dipole–dipole interactions, their estimation under periodic boundary conditions requires an efficient approximate algorithm. We chose the dipolar-P^{3}M method[65] for this purpose. The simulations were carried out using the package ESPResSo 3.3.1.[66,67]

3 Results and discussion

Below, we will first present the results of the experimental measurements of the magnetic hysteresis for three magnetic elastomers with different matrix stiffness and the same concentration of magnetically hard particles only. We show that the three systems exhibit the peculiar difference in the first magnetisation loop that we try to explain using computer simulations with the minimal model introduced above. These simulations indicate that irreversible relaxations of the translational and rotational constraints are essential for this effect to manifest. This observation is confirmed

by experimental microstructural analysis using micro-computed tomography.

3.1 Experimental magnetic measurements

The measurement of magnetisation loops is a standard method used to characterise the magnetic response of materials. In the experiments we measure three consecutive magnetisation loops on each sampled system in order to observe the differences between the first loop and the next ones.

Fig. 4 shows the experimental magnetisation loops obtained for three different samples of magnetic elastomer filled with a 5% in volume of NdFeB microparticles. The measurements were performed right after their synthesis. Fig. 4(a) corresponds to a sample with a tensile modulus of E = 30 kPa (SME1), whereas one of the samples in Fig. 4(b) (SME2) is E = 80 kPa and one of the samples in Fig. 4(c) (SME3) is E = 900 kPa. In order to ease the comparison with the simulation results, fields and magnetisations in these figures are normalised with their corresponding values at saturation, H_{max} and M_{max} respectively. For all samples the first magnitude was approximately $H_{max} \approx$ 1660 kA m^{-1}, whereas the saturation magnetisation of samples SME1 and SME3, $M_{max} \approx$ 38 kA m^{-1}, was slightly lower than that corresponding to sample SME2, $M_{max} \approx$ 50 kA m^{-1}.

In the case of SME1 and SME2 the area enclosed by the hysteresis loops is rather small due to the moderate stiffness of the matrix. For SME3 the area is larger due to the higher stiffness of the matrix. It can also be observed that the coercive fields corresponding to the upward and backward curves are not symmetric. This is caused by the internal interaction field due to the magnetisation of the particles.[68] Importantly, all samples show a significant difference in their first magnetisation loop with respect to the next ones, being particularly clear in the second half of the backward curves.

Also interesting is the fact that such a difference is more clear for sample SME2. The reason for this is the interplay between the particle–matrix coupling and the stiffness of the matrix itself. If the stiffness of the matrix is very low (SME1) the restoring forces of the matrix acting on the particles are low. The particles are able to rotate almost freely when an external magnetic field is applied. The latter results in a weaker asymmetric behaviour. If the stiffness of the matrix is too high (SME3), the particles are strongly constrained by the matrix and the rotations are hindered, causing a disappearance of the asymmetric behaviour. As a consequence, the largest asymmetry is observed for sample SME2, for which strong field induced rotations are possible. In this case the rotations might require a partial destruction of the coupling between the particles and the matrix.

For comparing the experimental results of the magnetisation and the simulation results, only SME1 and SME2 have been used due to the fact that almost no asymmetry was found for sample SME3.

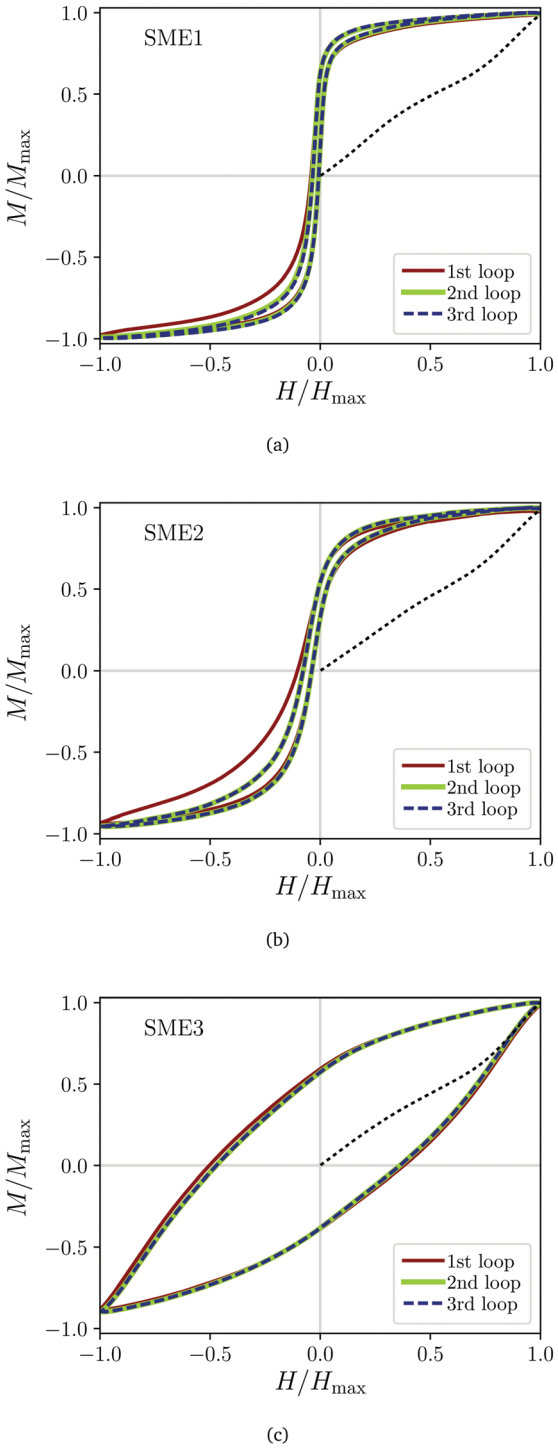

Fig. 4 First three normalised magnetisation loops obtained experimentally for samples of magnetic elastomers filled with a 5% in volume of NdFeB microparticles. The physical magnitudes of saturation field and magnetisation are given in the main text. In both plots the dotted line is the initial magnetisation curve (black), the thin solid line is the first magnetisation loop (red), the thick solid line is the second loop (green) and the dashed line is the third one (blue). Each figure corresponds to samples with different tensile modulus: (a) 30 kPa; (b) 80 kPa; (c) 900 kPa.

3.2 Magnetisation curves in simulations

We focus the discussion of the simulation results on the magnetisation loops obtained for the two models introduced in Section 2.2. All the simulations were performed for systems of N = 512 magnetic beads. In order to reduce the fluctuations

in the magnetisation curves led by the moderate size of the samples, for each system we averaged the results produced by three independent runs.

First, we present the simulation results corresponding to the case when no inelastic constraint relaxations are allowed, *i.e.*, when a fully elastic regime is simulated. Under these conditions, no difference between the first and next magnetisation loops has been observed in any simulated system. Inelastic deformations will be discussed afterwards.

3.2.1 Simulation results under elastic deformations. Fig. 5 shows several examples of normalised magnetisation loops obtained for model M1 with different concentrations of magnetic beads, ρ (Fig. 5(a)), and intervals of rigidities of the elastic constraints, K (Fig. 5(b)). In these plots the magnetisation is normalised by the maximum possible value that can be obtained according to the amount of particles and their reduced dipole moment, $M_{max} = N\mu = 1024$, whereas the maximum strength of the applied reduced field is in this case $H_{max} = 6$. Fig. 5(a) includes two snapshots that illustrate the typical arrangements of the magnetic beads under saturation conditions: we can observe the formation of chain-like aggregates with a high alignment of the dipoles with respect to the applied field. This figure also shows that the area enclosed by the magnetisation loops increases significantly with concentration. At a very low concentration, $\rho = 0.01$, not only does such an area become small, but also the profile of the loop shows kinks. The area of the loop also decreases as the rigidity of the springs increases. Since in the experiment the particles are magnetically hard, in the simulations the modulus of the magnetic moment of the particles is fixed. As a consequence, the profile of the loops is mirror-symmetric with respect to the magnetisation axis. Therefore, the upward and downward coercive fields are symmetric.

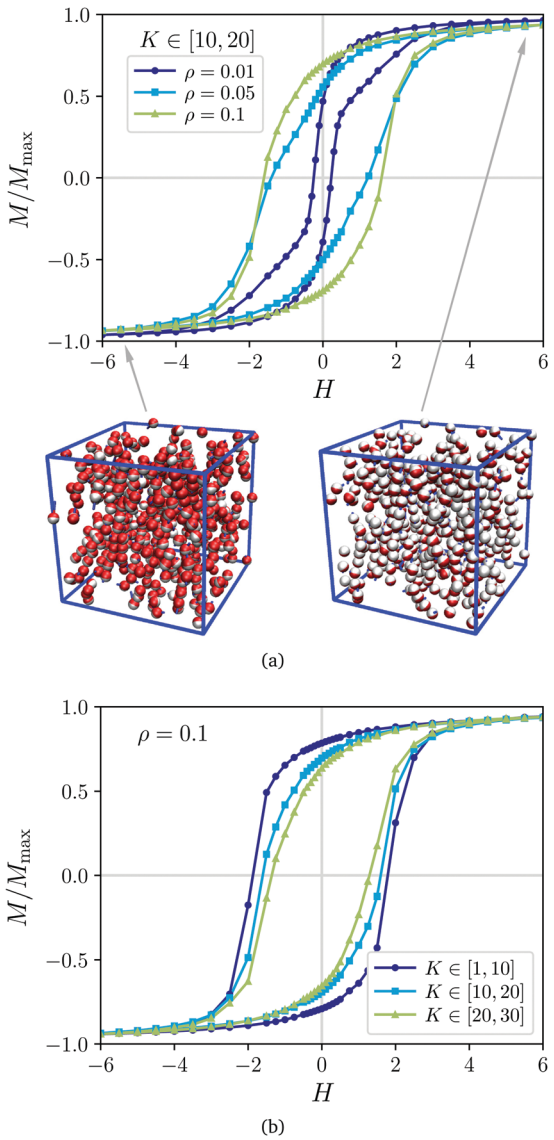

Fig. 5 Magnetisation loops obtained in simulations with elastic translational constraints (model M1) for a system of $N = 512$ particles with $\mu = 2$ and $T = 10^{-4}$: (a) for a fixed interval of spring rigidities, $K \in [10,20]$, and different densities. Snapshots of configurations corresponding to saturation conditions are included, with magnetic beads represented as spheres with two colour hemispheres that indicate the orientation of their dipoles. (b) For a fixed density, $\rho = 0.1$, and different intervals of spring rigidities.

Finally, some examples of the magnetisation measurements obtained for model M2 under different concentrations and spring rigidities are shown in Fig. 6. In this case, despite the maximum strength of the reduced field we sampled, $H_{max} = 15$ was much larger than the one applied to M1 systems, the effect of these elastic constraints is so strong that a significant hysteresis is only observed for M2 systems with the lowest sampled rigidities, $K \in [1,10]$.

After this overview of the elastic response of elastomer models M1 and M2, we can now discuss the effects of inelastic deformations in the next section.

3.2.2 Simulation results under first-loop inelastic deformations. We sampled several values of the shift probability within the ranges $0.01 \leq p_s \leq 0.4$, for M1, and $0.001 \leq p_s \leq 0.1$ for M2. For each system, we chose a maximum strength of the applied field, H_{max}, that gives at least 99% of the saturation magnetisation. For the rest of the system parameters the same values and intervals discussed above were used.

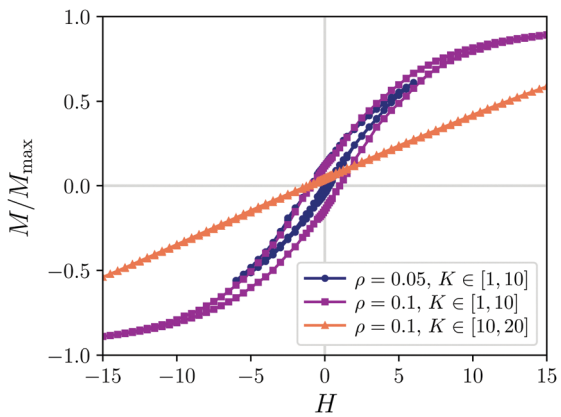

Fig. 6 Examples of magnetisation measurements obtained in simulations with elastic translational and rotational constraints (model M2) for a system of $N = 512$ particles with $\mu = 2$, $T = 10^{-4}$ and diverse combinations of particle concentrations and spring rigidity intervals.

Fig. 7 shows the simulation results of the first three normalised magnetisation loops obtained for M1 systems with $K \in [1,10]$, $p_s = 0.2$ and four different values of ρ. One can see that a notable difference in the first magnetisation loop with respect to the next ones only occurs for the lowest concentration: as ρ is increased, such differences tend to vanish and the loop profiles tend to have a large enclosed area, as corresponds to the low rigidity of the constraints. Significant differences for the first loop were not observed in any of the sampled M1 systems with higher rigidities. Moreover, a simple visual comparison of the difference observed at low ρ and K (Fig. 7(a)) shows that it is rather distinct from the ones obtained in the experiments (Fig. 4). Therefore, we can conclude that the model M1 does not provide a reasonably good qualitative representation of the experimental behaviour, at least within the broad ranges of the parameters we sampled.

The magnetic response of model M2 turns out to be much more affected by the inelastic deformations than that of M1. Fig. 8 and 9 show four selected results of the first three normalised magnetisation loops obtained from the M2 samples with $p_s = 0.002$ and different combinations of ρ and K. In contrast to Fig. 6, here in all cases clear hysteresis loops are obtained. Importantly, a clear difference in the first magnetisation loop with respect to the rest can be seen. This difference follows qualitatively quite well the experimental behaviour: the backward curve of the first loop shows moderately higher values of magnetisation than the subsequent ones along its lower half. Results for higher irreversible shift probabilities (not shown) indicate that the difference in the first loop tends to decrease as p_s increases. One can also observe that the area enclosed by the second and third loops, as expected, tends to decrease as the rigidity of the springs increases, but in this case the latter does not hinder the difference in the profile of the first loop. Three configuration snapshots included for the system with $\rho = 0.1$, $K \in [20,30]$ (Fig. 9(a)) illustrate the evolution of the constraining springs during the first loop: the initial configuration (top left) shows the random orientation of particles and springs and the initial stretching length of the latter; at the saturation field of the initial magnetisation curve (top right), the distance between the anchoring points of most particles has decreased significantly due to their irreversible shifts, allowing the

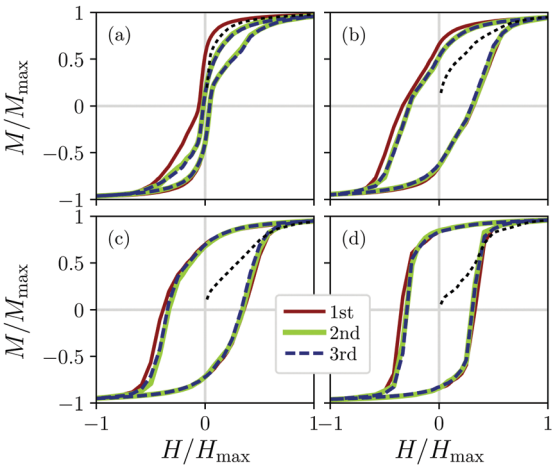

Fig. 7 Initial magnetisation curve (dotted black curve) and first three magnetisation loops obtained under initial inelastic deformations for the M1 samples composed of $N = 512$ magnetic beads, $\mu = 2$, $T = 10^{-4}$, $K \in [1,10]$, $p_s = 0.2$ and different densities: (a) $\rho = 0.01$, (b) $\rho = 0.03$, (c) $\rho = 0.05$, (d) $\rho = 0.1$.

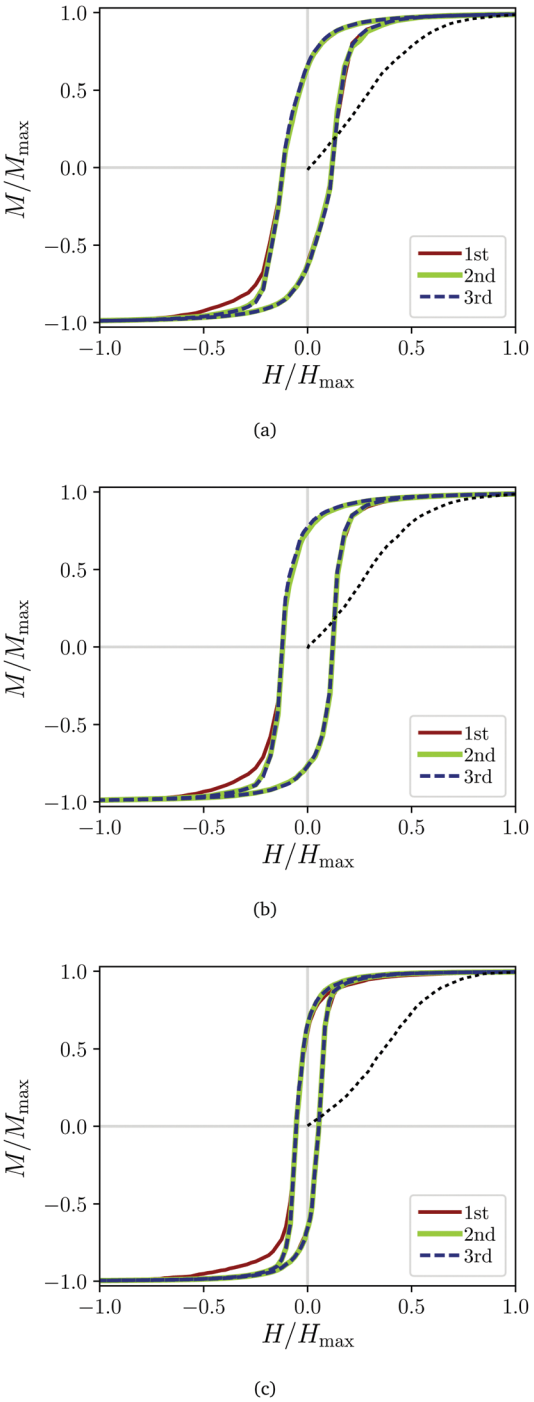

Fig. 8 Measurements of the initial magnetisation curve (dotted black curve) and first three magnetisation loops obtained for the model M2 samples with $N = 512$, $\mu = 2$, $T = 10^{-4}$ and $p_s = 0.002$, for different densities of the magnetic particles and rigidities of the springs: (a) $\rho = 0.05$, $K \in [1,10]$; (b) $\rho = 0.1$, $K \in [1,10]$; (c) $\rho = 0.1$, $K \in [10,20]$.

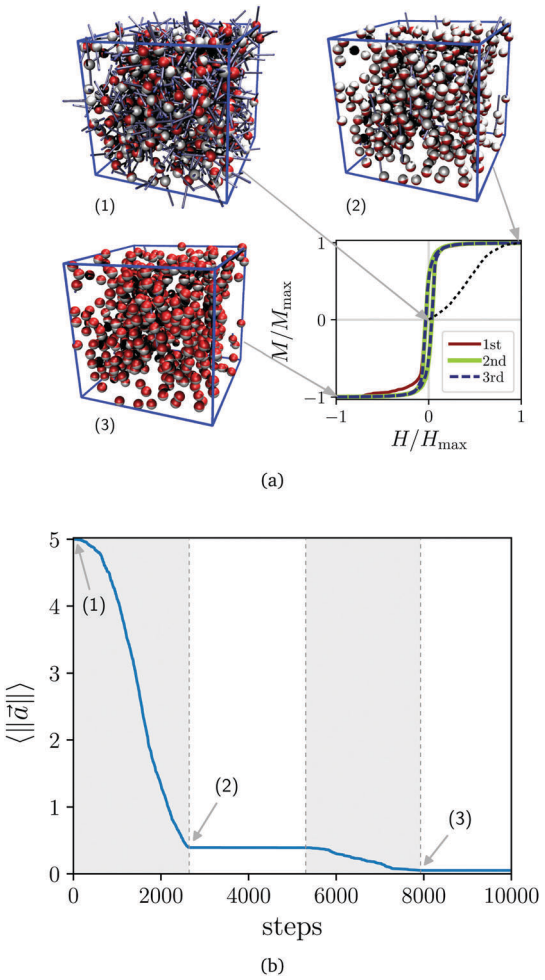

Fig. 9 (a) Initial magnetisation (dotted black curve) and the first three magnetisation loops measured for M2 samples with $\rho = 0.1$ and $K \in [20,30]$, together with three configuration snapshots corresponding to an initial configuration (1), a first saturation point (2) and a first inverted saturation point (3). Particles are represented as two colour spheres indicating the orientation of their dipole. Springs are represented as lines connecting the particles to the anchoring points. (b) Evolution of the average distance between the spring anchoring points of each particle, $\langle\|\vec{a}\|\rangle$, as a function of the measured steps along the first magnetisation loop. Darker background indicates those intervals where irreversible shifts were allowed. Numbers correspond to the points where the configuration snapshots shown in (a) were taken.

particles to highly align with the field and form chain-like aggregates; finally, after the first reverse saturation field is reached and the irreversible shifts are not allowed anymore, almost all pairs of anchoring points have largely reduced their separation to practically zero (bottom left), showing a configuration very similar to that observed for M1 under saturation. This evolution is better seen in Fig. 9(b), that shows an example of the change in the average distance between the anchoring points of the springs of each particle, $\langle\|\vec{a}\|\rangle$, as a function of the measured steps along the first magnetisation loop. Here we can see that during the first magnetisation of the system $\langle\|\vec{a}\|\rangle$ decreases notably, in a moderate way at the beginning and rather strongly afterwards, so that at the first saturation point its value is approximately 10% of the initial one. Finally, $\langle\|\vec{a}\|\rangle$ keeps decreasing during the first field inversion, reaching an almost zero value at the first inverse saturation point. After this, the system has become essentially identical to an M1 sample. According to what we found for M1 systems, the existence of eventual further shifts would not have any impact on the profile of subsequent magnetisation loops. A similar behaviour has been observed for any system that reproduces well the experimental difference in the first magnetisation loop.

Our results show that, despite its simplicity, model M2 with irreversible deformations represents rather well the experimental behaviour. This suggests that the translational and rotational constraints imposed by the polymer matrix on the embedded magnetic particles, as well as their irreversible relaxation due to field-induced deformations, play an important role in the difference observed experimentally for the first magnetisation loop of magnetic elastomers.

Below we verify this conclusion experimentally by means of direct observations of microstructural changes.

3.3 Experimental microstructural investigation

CT-scans were performed only for the SME2 sample due to both the time scales required by this method and the fact that this is the most interesting system as it exhibits the largest difference in its first magnetisation loop. For a better understanding of the microstructural changes induced by the field, we chose various points along the magnetisation curves to carry out CT scans, as detailed in Fig. 10. These CT scans are shown in Fig. 11. The first CT-scan was performed directly after the production of the sample (point 0 in Fig. 10). After that, a magnetic field of $B = 400$ mT was applied and a second CT scan of the sample was carried out (point 1 in Fig. 10). Afterwards, the sample was removed from the CT setup and exposed to a field $B = 2.2$ T for 30 minutes. Then the sample was placed back to the CT-setup at $B = 400$ mT field and one more scan was undertaken (point 2 in Fig. 10). This procedure was repeated first, with an inverted orientation of the fields (points 3 and 4 in Fig. 10), and with the original orientation of the fields (points 5 and 6 in Fig. 10). Finally, the last inversion of the field in the CT setup corresponds to point 7. The difference between the first

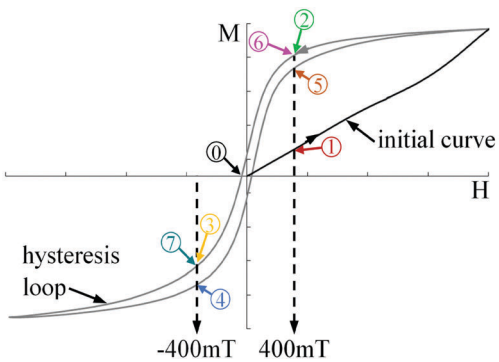

Fig. 10 Schematic representation of the different stages in which tomographic investigations of the sample have been undertaken. The different stages are highlighted in different colors with respect to the detailed views of the CT-scans in Fig. 11.

and the second magnetisation loops should manifest itself in deviations between points 2–6 and 3–7. As predicted by the magnetisation loops obtained in both the experiments and simulations, this difference should be more significant for points 3–7.

To ease the visualisation of the field-induced microstuctural changes, in Fig. 11 only a small part of the sample is shown. Applying a field of B = 400 mT and comparing this to the CT scan of the unmagnetised sample, the position of the particles changes only slightly, as seen in Fig. 11(a). This evidences a very strong initial mechanical coupling between the matrix and the magnetic particles. However, after the first positive saturation of the sample, as one can see in Fig. 11(b), most of the particles manage to align their longest major axis perpendicular to the magnetic field. In other words, the saturation field is strong enough to reduce the aforementioned coupling. It is worth mentioning that earlier X-ray diffraction measurements[35] have shown that the easy axis of these magnetically hard particles is the shortest major axis, so that the particles tend to rotate to orient their longest major axis perpendicular to the magnetic field. Particle rotations during the first inversion of the field, are again hindered by the matrix, that has to further deform in order to allow reorientation of the particles. From this point on, the particles are unconstrained enough to follow the field without the need of further irreversible deformations of the surrounding matrix, *i.e.*, field-induced rotations will only produce elastic deformations.

In order to provide a quantitative analysis of the reorientation occurring between points 2–6 and 3–7, visualised in Fig. 11(h) and (i),

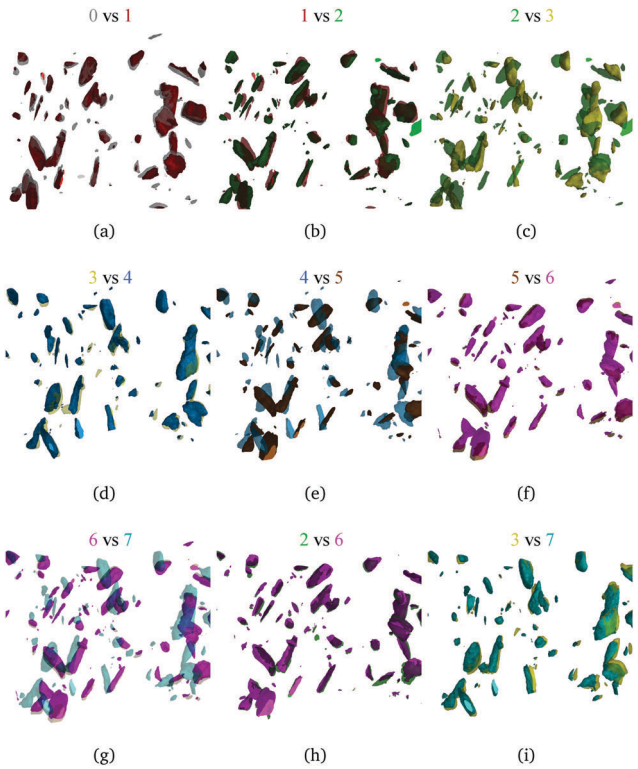

Fig. 11 Detailed views of CT Scans at different points of magnetisation which are explained in Fig. 10.

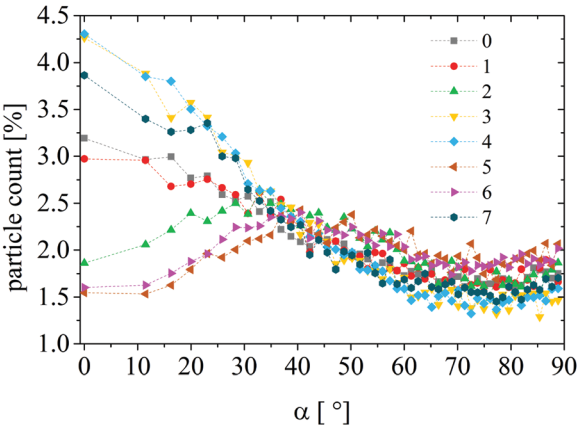

Fig. 12 Distribution of the angles between the major axis of the flake like NdFeB particles and the magnetic field direction for the different magnetisation states shown in Fig. 10.

we calculate the distributions of angles between particle long major axis and the field for all CT scans, averaged over approximately 45 000 particles, and plot them in Fig. 12. In our case, the angle of 90° corresponds to the alignment of particle magnetisation and the external field. One can see, that the initial distribution is basically uniform, with a slight bias towards perpendicular orientation of particles with respect to the vertical axis. Had the magnetisation process been totally reversible, the distributions of the angles for point 2 (green pointing up triangles in Fig. 12) and 6 (pink pointing right triangles in Fig. 12) and also for point 3 (yellow pointing down triangles in Fig. 12) and point 7 (teal circles in Fig. 12) would have been identical. However, we notice a clear difference between 2–6 and 3–7. These discrepancies can be attributed to the fact that the interaction forces between the matrix and particles during the first hysteresis loop are very high, so that some of the connections are destroyed. After that, the magnetisation will follow the same final hysteresis loop. In order to confirm this, CT-scans during the third and fourth magnetisation loops were carried out and no further evolution of the angular distribution was found. This additionally supports the protocol used in our computer simulations, in which the irreversible deformations were allowed only along the first field cycle.

4 Conclusions

In this work we present experimental evidence of a difference between the first and next magnetisation loops for SMEs made out of magnetically hard particles only. Importantly, to the best of our knowledge, until now this effect was reported only for hybrid SMEs with a mixture of magnetically soft and hard particles,[32] and no detailed explanation for it was found. Our experiments show that this difference depends non-monotonically on the interplay between the rigidity of the polymer matrix, its mechanical coupling with the particles, and the magnetic interactions in the system.

In order to understand the microstructural mechanism behind this behaviour, we put forward a minimal simulation

model of these materials that takes into account the rotational and/or translational constraints imposed by the matrix on the movement of the particles, as well as their relaxation due to field-induced irreversible deformations. Our simulations show that only when both types of constraints are acting and allowed to relax during the first magnetisation loop, the experimental difference is reproduced. This suggests that irreversible deformations of the matrix play a major part in this behaviour.

In order to confirm the conclusions drawn from the theoretical approach, we performed CT scans at different field strengths and various magnetisation loops. Direct observations of the changes in the microstructure allowed us to quantify the angular distributions of the particles with respect to the field direction at different stages of the magnetisation measurements. These distributions revealed a clear difference in the rotation of the particles for the first magnetisation loop: initially, particles turned to be strongly constrained by the matrix; after the first field inversion, only partial reorientation of the particles was observed; after the second field inversion and subsequent saturation of the samples, the rotations induced by further field cycles become fully reversible and the profile of the magnetisation loops does not change anymore. In other words, even though CT scans cannot directly provide the information about irreversible deformations of the matrix, the indications found from angular distributions and magnetisation measurements, combined with computer simulations, provide a clear picture of their role.

This study is the first step towards the profound understanding of the complex magnetic response of soft magnetic elastomers, that is totally essential for their technological applications. Besides that, being able to predict particle–particle and particle–matrix interactions in these systems, depending on composition and external stimuli, will allow the creation of materials with tunable macroscopic behaviours. That is why our next step is to clarify the part of the unavoidable particle polydispersity and shape anisotropy in the properties of SMEs by extending our experimental and theoretical approaches.

Conflicts of interest

There are no conflicts to declare.

Acknowledgements

This research was supported by the DFG grant OD 18/24-1 and DFG-RFBR grant 16-52-12008 within PAK907. The authors also acknowledge support from the Ministry of Education and Science of the Russian Federation, Contract 02.A03.21.0006 (Project 3.1438.2017/4.6). P. A. S. and S. S. K. are also supported by the FWF START-Projekt Y 627-N27. S. S. K. also acknowledges support from ETN-COLLDENSE (H2020-MSCA-ITN-2014, Grant No. 642774). Computer simulations were carried out at the Vienna Scientific Cluster.

References

1 G. Filipcsei, I. Csetneki, A. Szilágyi and M. Zrínyi, Magnetic Field-Responsive Smart, *Oligomers – Polymer Composites – Molecular Imprinting, Polymer Composites*, Springer Berlin Heidelberg, Berlin, Heidelberg, 2007, pp. 137–189.
2 J. Thévenot, H. Oliveira, O. Sandre and S. Lecommandoux, Magnetic responsive polymer composite materials, *Chem. Soc. Rev.*, 2013, **42**, 7099–7116.
3 S. Odenbach, Microstructure and rheology of magnetic hybrid materials, *Arch. Appl. Mech.*, 2016, **86**, 269–279.
4 T. Shiga, A. Okada and T. Kurauchi, Magnetroviscoelastic behavior of composite gels, *J. Appl. Polym. Sci.*, 1995, **58**(4), 787–792.
5 M. Zrínyi, Intelligent polymer gels controlled by magnetic fields, *Colloid Polym. Sci.*, 2000, **278**(2), 98–103.
6 S. Reinicke, S. Dohler, S. Tea, M. Krekhova, R. Messing, A. M. Schmidt and H. Schmalz, Magneto-responsive hydrogels based on maghemite/triblock terpolymer hybrid micelles, *Soft Matter*, 2010, **6**, 2760–2773.
7 N. Frickel, R. Messing and A. M. Schmidt, Magneto-mechanical coupling in cofe2o4-linked paam ferrohydrogels, *J. Mater. Chem.*, 2011, **21**, 8466–8474.
8 R. Messing, N. Frickel, L. Belkoura, R. Strey, H. Rahn, S. Odenbach and A. M. Schmidt, Cobalt ferrite nanoparticles as multifunctional cross-linkers in paam ferrohydrogels, *Macromolecules*, 2011, **44**(8), 2990–2999.
9 I. Patrick, Stimuli-responsive hydrogels cross-linked by magnetic nanoparticles, *Soft Matter*, 2013, **9**, 3465–3468.
10 Y. Xu, X. Gong and S. Xuan, Soft magnetorheological polymer gels with controllable rheological properties, *Smart Mater. Struct.*, 2013, **22**(7), 964–1726.
11 L. Roeder, P. Bender, M. Kundt, A. Tschope and A. M. Schmidt, Magnetic and geometric anisotropy in particle-crosslinked ferrohydrogels, *Phys. Chem. Chem. Phys.*, 2015, **17**, 1290–1298.
12 M. R. Jolly, J. D. Carlson, B. C. Muñoz and T. A. Bullions, The magnetoviscoelastic response of elastomer composites consisting of ferrous particles embedded in a polymer matrix, *J. Intell. Mater. Syst. Struct.*, 1996, **7**(6), 613–622.
13 J. M. Ginder, M. E. Nichols, L. D. Elie and J. L. Tardiff, Magnetorheological elastomers: properties and applications, in *Smart Structures and Materials 1999: Smart Materials Technologies*, ed. M. R. Wuttig, Proceedings SPIE, SPIE, 1999, vol. 3675, pp. 131–138.
14 J. D. Carlson and M. R. Jolly, Mr fluid, foam and elastomer devices, *Mechatronics*, 2000, **10**, 555–569.
15 Z. Varga, G. Filipcsei and M. Zrínyi, Magnetic field sensitive functional elastomers with tuneable elastic modulus, *Polymer*, 2006, **47**(1), 227–233.
16 A. Fuchs, Q. Zhang, J. Elkins, F. Gordaninejad and C. Evrensel, Development and characterization of magnetorheological elastomers, *J. Appl. Polym. Sci.*, 2007, **105**(5), 2497–2508.
17 A. V. Chertovich, G. V. Stepanov, E. Yu. Kramarenko and A. R. Khokhlov, New composite elastomers with giant magnetic response, *Macromol. Mater. Eng.*, 2010, **295**(4), 336–341.

18 A. Boczkowska and S. Awietjan, Microstructure and properties of magnetorheological elastomers, in *Advanced Elastomers – Technology, Properties and Applications*, ed. A. Boczkowska, InTech, Rijeka, 2012, ch. 6.
19 Z. Varga, J. Fehér, G. Filipcsei and M. Zrínyi, Smart nanocomposite polymer gels, *Macromol. Symp.*, 2003, **200**, 93–100.
20 H.-X. Deng, X.-L. Gong and L.-H. Wang, Development of an adaptive tuned vibration absorber with magnetorheological elastomer, *Smart Mater. Struct.*, 2006, **15**(5), N111.
21 T. L. Sun, X. L. Gong, W. Q. Jiang, J. F. Li, Z. B. Xu and W. H. Li, Study on the damping properties of magnetorheological elastomers based on *cis*-polybutadiene rubber, *Polym. Test.*, 2008, **27**(4), 520–526.
22 W. Li and X. Zhang, Research and applications of mr elastomers, *Recent Pat. Mech. Eng.*, 2008, **1**, 161–166.
23 H. Böse, R. Rabindranath and J. Ehrlich, Soft magnetorheological elastomers as new actuators for valves, *J. Intell. Mater. Syst. Struct.*, 2012, **23**(9), 989–994.
24 W. H. Li, X. Z. Zhang and H. Du, Magnetorheological Elastomers and Their Applications, *Advanced Structured Materials*, Springer Berlin Heidelberg, Berlin, Heidelberg, 2013, vol. 11, pp. 357–374.
25 Y. Li, J. Li, W. Li and H. Du, A state-of-the-art review on magnetorheological elastomer devices, *Smart Mater. Struct.*, 2014, **23**(12), 123001.
26 S. Odenbach, Ferrofluids, in *Handbook of Magnetic Materials*, ed. K. H. J. Buschow, Elsevier, 2006, ch. 3, vol. 16, pp. 127–208.
27 J. de Vicente, D. J. Klingenberg and R. Hidalgo-Alvarez, Magnetorheological fluids: a review, *Soft Matter*, 2011, **7**, 3701–3710.
28 B. Holger, Viscolelastic properties of silicone based magnetorheological elastomers, *Int. J. Mod. Phys. B*, 2007, **21**, 4790–4797.
29 T. Gundermann and S. Odenbach, Investigation of the motion of particles in magnetorheological elastomers by Xμ-CT, *Smart Mater. Struct.*, 2014, **23**(10), 105013.
30 O. V. Stolbov, Y. L. Raikher and M. Balasoiubc., Modelling of magnetodipolar striction in soft magnetic elastomers, *Soft Matter*, 2011, **7**, 8484–8487.
31 G. V. Stepanov, D. Y. Borin, Y. L. Raikher, P. V. Melenev and N. S. Perov, Motion of ferroparticles inside the polymeric matrix in magnetoactive elastomers, *J. Phys.: Condens. Matter*, 2008, **20**, 204121.
32 J. M. Linke, D. Yu. Borin and S. Odenbach, First-order reversal curve analysis of magnetoactive elastomers, *RSC Adv.*, 2016, **6**, 100407–100416.
33 G. V. Stepanov, D. Yu Borin, A. V. Bakhtiiarov and P. A. Storozhenko, Magnetic properties of hybrid elastomers with magnetically hard fillers: rotation of particles, *Smart Mater. Struct.*, 2017, **26**(3), 035060.
34 K. A. Kalina, J. Brummund, P. Metsch, M. Kästner, D. Y. Borin, J. M. Linke and S. Odenbach, Modeling of magnetic hystereses in soft MREs filled with NdFeB particles, *Smart Mater. Struct.*, 2017, **26**, 105019.
35 M. Schümann, D. Y. Borin, S. Huang, G. K. Auernhammer, R. Müller and S. Odenbach, A characterisation of the magnetically induced movement of ndfeb-particles in magnetorheological elastomers, *Smart Mater. Struct.*, 2017, **26**(9), 095018.
36 D. Günther, D. Yu. Borin, S. Günther and S. Odenbach, X-ray micro-tomographic characterization of field-structured magnetorheological elastomers, *Smart Mater. Struct.*, 2012, **21**(1), 015005.
37 T. Borbáth, S. Günther, D. Y. Borin, Th. Gundermann and S. Odenbach, Xμ-CT analysis of magnetic field-induced phase transitions in magnetorheological elastomers, *Smart Mater. Struct.*, 2012, **21**(10), 105018.
38 M. Schümann and S. Odenbach, *In situ* observation of the particle microstructure of magnetorheological elastomers in presence of mechanical strain and magnetic fields, *J. Magn. Magn. Mater.*, 2017, **441**, 88–92.
39 T. Gundermann, P. Cremer, H. Löwen, A. M. Menzel and S. Odenbach, Statistical analysis of magnetically soft particles in magnetorheological elastomers, *Smart Mater. Struct.*, 2017, **26**(4), 045012.
40 T. Gundermann, S. Günther, D. Borin and S. Odenbach, A comparison between micro- and macro-structure of magnetoactive composites, *J. Phys.: Conf. Ser.*, 2013, **412**(1), 012027.
41 R. C. González, R. E. Woods and S. L. Eddins, *Digital Image Processing Using MATLAB*, Prentice Hall Press, Englewood Cliffs, NJ, USA, 2014.
42 E. Jarkova, H. Pleiner, H.-W. Müller and H. R. Brand, Hydrodynamics of isotropic ferrogels, *Phys. Rev. E: Stat., Nonlinear, Soft Matter Phys.*, 2003, **68**, 041706.
43 S. Bohlius, H. R. Brand and H. Pleiner, Macroscopic dynamics of uniaxial magnetic gels, *Phys. Rev. E: Stat., Nonlinear, Soft Matter Phys.*, 2004, **70**, 061411.
44 A. Yu. Zubarev, On the theory of the magnetic deformation of ferrogels, *Soft Matter*, 2012, **8**, 3174–3179.
45 D. Romeis, V. Toshchevikov and M. Saphiannikova, Elongated micro-structures in magneto-sensitive elastomers: a dipolar mean field model, *Soft Matter*, 2016, **12**, 9364–9376.
46 D. Romeis, P. Metsch, M. Kästner and M. Saphiannikova, Theoretical models for magneto-sensitive elastomers: a comparison between continuum and dipole approaches, *Phys. Rev. E*, 2017, **95**, 042501.
47 M. R. Dudek, B. Grabiec and K. W. Wojciechowski, Molecular dynamics simulations of auxetic ferriteogel, *Rev. Adv. Mater. Sci.*, 2007, **14**(2), 167–173.
48 D. S. Wood and P. J. Camp, Modeling the properties of ferrogels in uniform magnetic fields, *Phys. Rev. E: Stat., Nonlinear, Soft Matter Phys.*, 2011, **83**, 011402.
49 D. Ivaneyko, V. P. Toshchevikov, M. Saphiannikova and G. Heinrich, Magneto-sensitive elastomers in a homogeneous magnetic field: a regular rectangular lattice model, *Macromol. Theory Simul.*, 2011, **20**(6), 411–424.
50 M. A. Annunziata, A. M. Menzel and H. Löwen, Hardening transition in a one-dimensional model for ferrogels, *J. Chem. Phys.*, 2013, **138**(20), 204906.
51 G. Pessot, P. Cremer, D. Y. Borin, S. Odenbach, H. Löwen and A. M. Menzel, Structural control of elastic moduli in ferrogels and the importance of non-affine deformations, *J. Chem. Phys.*, 2014, **141**(12), 124904.

52 M. Tarama, P. Cremer, D. Y. Borin, S. Odenbach, H. Löwen and A. M. Menzel, Tunable dynamic response of magnetic gels: impact of structural properties and magnetic fields, *Phys. Rev. E: Stat., Nonlinear, Soft Matter Phys.*, 2014, **90**, 042311.
53 D. Ivaneyko, V. Toshchevikov and M. Saphiannikova, Dynamic moduli of magneto-sensitive elastomers: a coarse-grained network model, *Soft Matter*, 2015, **11**, 7627–7638.
54 G. Pessot, H. Löwen and A. M. Menzel, Dynamic elastic moduli in magnetic gels: normal modes and linear response, *J. Chem. Phys.*, 2016, **145**(10), 104904.
55 R. Weeber, S. Kantorovich and C. Holm, Deformation mechanisms in 2d magnetic gels studied by computer simulations, *Soft Matter*, 2012, **8**, 9923–9932.
56 R. Weeber, S. Kantorovich and C. Holm, Ferrogels cross-linked by magnetic nanoparticles – deformation mechanisms in two and three dimensions studied by means of computer simulations, *J. Magn. Magn. Mater.*, 2015, **383**, 262–266.
57 A. V. Ryzhkov, P. V. Melenev, C. Holm and Yu. L. Raikher, Coarse-grained molecular dynamics simulation of small ferrogel objects, *J. Magn. Magn. Mater.*, 2015, **383**, 277–280.
58 A. V. Ryzhkov, P. V. Melenev, M. Balasoiu and Y. L. Raikher, Structure organization and magnetic properties of micro-scale ferrogels: the effect of particle magnetic anisotropy, *J. Chem. Phys.*, 2016, **145**(7), 074905.
59 J. D. Weeks, D. Chandler and H. C. Andersen, Role of repulsive forces in determining the equilibrium structure of simple liquids, *J. Chem. Phys.*, 1971, **54**(12), 5237–5247.
60 J. J. Cerdà, P. A. Sánchez, T. Sintes and C. Holm, Phase diagram for a single flexible Stockmayer polymer at zero field, *Soft Matter*, 2013, **9**, 7185–7195.
61 P. A. Sánchez, J. J. Cerdà, T. Sintes and C. Holm, Effects of the dipolar interaction on the equilibrium morphologies of a single supramolecular magnetic filament in bulk, *J. Chem. Phys.*, 2013, **139**, 044904.
62 D. Frenkel and B. Smit, *Understanding molecular simulation*, Academic Press, 2002.
63 J. J. Cerdà, S. Kantorovich and C. Holm, Aggregate formation in ferrofluid monolayers: simulations and theory, *J. Phys.: Condens. Matter*, 2008, **20**, 204125.
64 S. Kantorovich, J. J. Cerdà and C. Holm, Microstructure analyisis of monodisperse ferrofluid monolayers: theory and simulation, *Phys. Chem. Chem. Phys.*, 2008, **10**, 1883–1895.
65 J. J. Cerdà, V. Ballenegger, O. Lenz and C. Holm, P3m algorithm for dipolar interactions, *J. Chem. Phys.*, 2008, **129**, 234104.
66 H. J. Limbach, A. Arnold, B. A. Mann and C. Holm, ESPResSo – an extensible simulation package for research on soft matter systems, *Comput. Phys. Commun.*, 2006, **174**(9), 704–727.
67 A. Arnold, O. Lenz, S. Kesselheim, R. Weeber, F. Fahrenberger, D. Roehm, P. Košovan and C. Holm, Espresso 3.1: molecular dynamics software for coarse-grained models, in *Meshfree Methods for Partial Differential Equations VI*, ed. M. Griebel and M. A. Schweitzer, Lecture Notes in Computational Science and Engineering, Springer, Berlin Heidelberg, 2013, vol. 89, pp. 1–23.
68 A. P. Roberts, D. Heslop, X. Zhao and C. R. Pike, Understanding fine magnetic particle systems through use of first-order reversal curve diagrams, *Rev. Geophys.*, 2014, **52**(4), 557–602.